



Frequency and  
Trends of  
Above-Cloud  
Aerosols

R. Alfaro-Contreras et al.

This discussion paper is/has been under review for the journal Atmospheric Chemistry and Physics (ACP). Please refer to the corresponding final paper in ACP if available.

# Investigating the frequency and trends in global above-cloud aerosol characteristics with CALIOP and OMI

R. Alfaro-Contreras<sup>1</sup>, J. Zhang<sup>1</sup>, J. R. Campbell<sup>2</sup>, and J. S. Reid<sup>2</sup>

<sup>1</sup>Department of Atmospheric Science, University of North Dakota, Grand Forks, ND, USA

<sup>2</sup>Marine Meteorology Division, Naval Research Laboratory, Monterey, CA, USA

Received: 12 January 2015 – Accepted: 20 January 2015 – Published: 17 February 2015

Correspondence to: J. Zhang (jzhang@atmos.und.edu)

Published by Copernicus Publications on behalf of the European Geosciences Union.

Title Page

Abstract

Introduction

Conclusions

References

Tables

Figures



Back

Close

Full Screen / Esc

Printer-friendly Version

Interactive Discussion



## Abstract

Seven and a half years (June 2006–November 2013) of Cloud-Aerosol Lidar with Orthogonal Polarization (CALIOP) aerosol and cloud layer products are compared with collocated Ozone Monitoring Instrument (OMI) Aerosol Index (AI) data and Aqua Moderate Resolution Imaging Spectroradiometer (MODIS) cloud products, to investigate variability in estimates of bi-annual and monthly above-cloud aerosol (ACA) events globally. The active- (CALIOP) and passive-based (OMI-MODIS) techniques have their advantages and caveats for ACA detection, and thus both are used to get a thorough and robust comparison of daytime cloudy-sky ACA distribution and climatology. For the first time, baseline above-cloud aerosol optical depth (ACAOD) and AI thresholds are derived and examined ( $AI = 1.0$ ,  $ACAOD = 0.015$ ) for each sensor. Both OMI-MODIS and CALIOP-based daytime spatial distributions of ACA events show similar patterns during both study periods (December–May) and (June–November). Divergence exists in some regions, however, such as Southeast Asia during June through November, where daytime cloudy-sky ACA frequencies of up to 10 % are found from CALIOP yet are non-existent from the OMI-based method. Conversely, annual cloudy-sky ACA frequencies of 20–30 % are reported over Northern Africa from the OMI-based method, yet are largely undetected by the CALIOP-based method. This is possibly due to a misclassification of thick dust plumes as clouds by the OMI-MODIS based method. An increasing trend of  $\sim 0.5\%$  per year (since 2009) in global monthly cloudy-sky ACA daytime frequency of occurrence is found using the OMI-MODIS based method. Yet, CALIOP-based global daytime ACA frequencies exhibit a near-zero trend. Further analysis suggests that the OMI derived cloudy-sky ACA frequency trend may be affected by OMI row anomalies in later years. A few regions are found to have increasing trends of cloudy-sky ACA frequency, including the Middle-East and India. Regions with slightly negative cloudy-sky ACA frequency trends are found over South America and the Southern Oceans, while remaining regions in the study show a near-zero trend. Global and regional trends are not statistically significant, though, given relatively lacking sam-

## Frequency and Trends of Above-Cloud Aerosols

R. Alfaro-Contreras et al.

Title Page

Abstract

Introduction

Conclusions

References

Tables

Figures



Back

Close

Full Screen / Esc

Printer-friendly Version

Interactive Discussion





## Frequency and Trends of Above-Cloud Aerosols

R. Alfaro-Contreras et al.

[Title Page](#)[Abstract](#)[Introduction](#)[Conclusions](#)[References](#)[Tables](#)[Figures](#)[◀](#)[▶](#)[◀](#)[▶](#)[Back](#)[Close](#)[Full Screen / Esc](#)[Printer-friendly Version](#)[Interactive Discussion](#)

element is essential for decoupling aerosol and cloud scattering contributions in ACA events (Devasthale and Thomas, 2011). Utilizing four years of CALIOP Level 2 data (Winker et al., 2009), Devasthale and Thomas (2011) evaluated seasonal and latitudinal patterns of ACA for liquid water cloud events. Alfaro-Contreras et al. (2014) describe seasonal frequencies in ACA over the southern Atlantic Ocean off the West African coastline as well as over the Gulf of Tonkin in Southeast Asia where high ACA loading episodes were found during the summer and fall months and early spring months, respectively.

Whereas limited process studies have helped raise awareness of the ACA problem overall, trends in global ACA frequency distribution have not yet been developed with CALIOP. Despite a nearly eight-year (2006–present) CALIOP data archive available, one must be considerate of the fact that satellite lidar profiling is constrained presently to a single laser-illuminated curtain and roughly sixteen daily orbits of the planet. Questions thus arise about the representativeness of CALIOP datasets for some climatological analyses, like ACA, given its temporal persistence and spatial extent (Devasthale and Thomas, 2011; Yu et al., 2012). Additionally, for CALIPSO-based ACA studies, and especially trends, to be meaningful, the potential impacts of signal deterioration to CALIOP derived aerosol optical depth (AOD) values need to be known. Despite the practical limitations of applying passive sensors for studying phenomena like ACA, then, the relatively wide field-of-view on passive imagers renders far greater data volume, which makes them more ideal options for a long-term study.

Ozone Monitoring Instrument (OMI) measurements have also been used for studying ACA events (e.g., Wilcox et al., 2009; Yu et al., 2012; Alfaro-Contreras et al., 2014). In particular, the OMI Aerosol Index (AI), computed using the difference between observed and calculated ultraviolet (UV) radiances (Torres et al., 2007), has been used to locate UV-absorbing aerosols suspended over bright cloud decks (e.g. Yu et al., 2012; Torres et al., 2012). This technique, originally used on the Total Ozone Mapping Spectrometer (TOMS), can only be used to detect UV-absorbing aerosols, such as biomass burning smoke and desert dust aerosols and is sensitive to underneath

cloud properties (e.g. Yu et al., 2012; Alfaro-Contreras et al., 2014). Further and compared with CALIOP, OMI measurements represent a relatively large surface footprint of 13 km  $\times$  24 km at nadir, which limits cloud-clearing efficacies since footprints of this size are prone to sub-pixel cloud contamination (Torres et al., 2007). Collocated Moderate Resolution Imaging Spectroradiometer (MODIS) observations, however, as part of NASA's A-Train satellite constellation, which includes CALIOP (Stephens et al., 2002), can be utilized to distinguish and filter cloudy pixels/scenes within the OMI footprint.

Comparison of active vs. passive based sensors for evaluating the spatio-temporal coverage of ACA events, and for studying regional and global trends of ACA occurrence, represents a conservative means for conceptualizing the breadth of the problem. The goal of this work is, therefore, to compare and contrast distributions in global and regional ACA frequencies and their apparent trends using both CALIOP- and OMI-based approaches. Caveats to each approach are specifically identified, and thus qualified within the discussion so as to keep comparison as consistent and robust as possible. We highlight regions particularly susceptible to ACA occurrence, establishing a baseline for future ACA-induced biases in satellite cloud property retrievals overall.

## 2 Datasets and methodology

CALIOP Level 2 5 km cloud and aerosol layer products (Winker et al., 2010) and OMI Level 2 Collection 3 UV aerosol products (OMAERUV; Torres et al., 2007) are paired with Aqua MODIS cloud products (MYD06\_L2; King et al., 1997) and Aerosol Robotic Network (AERONET; Holben et al., 1998) Level 2.0 Version 2 cloud-screened data from June 2006 through November 2013.

For identification of ACA, 5 km CALIOP 532 nm cloud and aerosol layer products are used (Winker et al., 2009, 2010) for resolving aerosol extinction above apparent cloud top heights in each respective product file (e.g. Yu et al., 2012; Alfaro-Contreras et al., 2014). The 532 nm above-cloud aerosol optical depth (ACAOD) is then solved by integrating the extinction coefficient over those corresponding bins (Liu et al., 2013;

### Frequency and Trends of Above-Cloud Aerosols

R. Alfaro-Contreras et al.

Title Page

Abstract

Introduction

Conclusions

References

Tables

Figures



Back

Close

Full Screen / Esc

Printer-friendly Version

Interactive Discussion



## Frequency and Trends of Above-Cloud Aerosols

R. Alfaro-Contreras et al.

[Title Page](#)[Abstract](#)[Introduction](#)[Conclusions](#)[References](#)[Tables](#)[Figures](#)[Back](#)[Close](#)[Full Screen / Esc](#)[Printer-friendly Version](#)[Interactive Discussion](#)

Kacenelebogen et al., 2014). The CALIOP-based trend analysis may be affected by CALIOP signal deterioration over time. Thus, collocated AERONET datasets are used, as the first order approximation, for evaluating instrument-related variations in the long term CALIOP AOD trend. Reported at eight spectral bands ranging from 0.34–1.64  $\mu\text{m}$  (Holben et al., 1998), AERONET AOD datasets are frequently used for validating satellite retrievals (e.g., Zhang et al., 2001; Yu et al., 2003; Kaufman et al., 2005a; Remer et al., 2005; Hahn et al., 2010; Shi et al., 2011; Sayer et al., 2012), as well as model simulated aerosol optical properties (e.g. Zhang et al., 2011, 2014).

The Level 2.0 cloud-screened and quality-assured AERONET AOD data (Eck et al., 1999) from all available coastal and island AERONET sites are used for collocating with CALIOP data. AERONET AOD data are interpolated, based on a method described in Zhang and Reid (2006), to the 0.532  $\mu\text{m}$ , which is the wavelength for CALIOP reported AODs, and are spatio-temporally-collocated with CALIOP AOD data. Instrument-related trends in the CALIOP AOD are investigated by calculating the global monthly-mean AERONET and CALIOP AODs and comparing the two monthly aerosol loading averages. CALIOP observations found to be within  $0.3^\circ$  latitude/longitude and  $\pm 30$  min of corresponding AERONET observations are considered collocated in space and time. In addition, we have used only pairs that have collocated AERONET AOD (0.532  $\mu\text{m}$ ) data less than 0.2 to exclude major aerosol episodes of continental origin. One additional quality assurance step is applied to exclude pairs with CALIOP AOD of larger than 0.6 for removing potentially noisy CALIOP data. In the case where several CALIOP observations are paired up with a single AERONET retrieval, a one-to-one relationship is established with the closest CALIOP observation.

Besides CALIOP data, OMI AI is used to isolate ACA events in those data. OMI AI and MODIS cloud datasets are spatio-temporally-collocated, given their position in the NASA “A-Train” constellation (e.g. Stephens et al., 2002), by collocating the two products with respect to overpass times and then identifying all temporally collocated cloudy MODIS pixels located within the boundaries of the OMI footprint. Such methods are described further in Alfaro-Contreras et al. (2014). Cloud fractions from the

## Frequency and Trends of Above-Cloud Aerosols

R. Alfaro-Contreras et al.

Title Page

Abstract

Introduction

Conclusions

References

Tables

Figures



Back

Close

Full Screen / Esc

Printer-friendly Version

Interactive Discussion



MODIS MYD06 product, reported at a 5 km horizontal resolution, are then leveraged for sub-pixel cloud clearing of the OMI AI. The MODIS cloud fraction is computed from the percentage of cloudy 1 km cloud mask product (MOD35) pixels within a given 5 km scene (e.g., Ackerman et al., 1998). With the exception of the cloud-top height restriction from the CALIOP data set, OMI/MODIS and CALIOP data are each filtered and quality-assured (described in detail in Alfaro-Contreras et al., 2014) to calculate respective global ACA distributions. It is known that that the OMI instrument experienced row anomalies beginning in 2008–2009 (<http://www.knmi.nl/omi/research/product/>, accessed on 22 December 2014). Thus the impact of the row anomalies to OMI AI trends is explored later in this paper.

### 3 Above-cloud aerosol baselines and limitations

There are always aerosol particles above clouds (a fact that quickly becomes lost when discussing the basic physics of ACA relative to satellite observation). Therefore, there exists some baseline thresholds by which active backscatter and/or passive radiances become significant relative to a given physical process or retrieval (i.e., radiative forcing, heating rates, transmission estimates, cloud microphysical retrievals, etc.). Accordingly, each of the instruments subject to the ACA phenomenon in this study exhibit fundamental sensitivities to ACA detection, which impact our ability to characterize the problem fully. Therefore, the baseline thresholds for significant ACA events need to be identified for both OMI- and CALIOP-based ACA studies.

To conceptualize the problem, shown in Fig. 1a are global distributions of mean CALIOP-derived daytime underlying cloud-top height for ACAOD events with optical thickness greater than zero. Figure 1b shows the averaged cloud-top height distributions of the highest cloud located within an atmospheric column regardless of the CALIOP ACAOD. Figure 1c and d depicts the same information as Fig. 1a and b, respectively, during the nighttime analysis. Globally averaged daytime cloud-top heights derived for each method, Fig. 1a and b, are  $\sim 2.0$  and 7.5 km, respectively. Clearly,



applying the CALIOP ACAOD  $> 0$  threshold makes a drastic change in the averaged cloud-top height. Considering that aerosol particles are always present above clouds, thus, results from Fig. 1 may indicate a limitation in CALIOP for detecting very optically thin aerosol particles (e.g. AOD  $< 0.01$ ).

5 Still, given the mean cloud-top height as shown in Fig. 1, we consider the unique AERONET site at Mauna Loa, Hawaii (LAT/LON, 3397 m above mean sea level). This free-tropospheric ground site rests at an altitude roughly within the global mean cloud-top heights discussed previously. Indeed, this physical feature of the site (that is being above the cloud deck below) is one of the key reasons for the importance of the site globally. The yearly mean Level 2.0 AERONET AOD (500 nm) there ranges from 10 0.013–0.023 from 1996–2013, and provides a generalized estimate for potential baseline ACAOD value globally. Kacenelenbogen et al. (2014) report that the CALIOP lidar exhibits limitations in detecting ACA plumes with ACAOD less than 0.02. This lower value may, therefore, represent an effective noise floor, whereby CALIOP algorithm response below it is compromised.

15 Based on Kacenelenbogen et al. (2014) as well as the AOD climatology from the Mauna Loa AERONET site analyses, we arbitrarily set the baseline CALIOP ACAOD value to 0.015. Considering the CALIOP ACAOD baseline is somewhat arbitrarily chosen, we investigate the CALIOP-based ACA frequency distributions by varying the baseline values to 0, 0.01, 0.015 and 0.02 as shown in Fig. 2. Figure 2a–d shows the cloudy-sky global ACA frequency distribution, defined as the number of scenes with AOD greater than our baseline values resolved a top a cloud of optical thickness greater than 0 divided by the number of scenes with column cloud optical depth (COD) greater than 0 per latitude and longitude bin, for the December–May period, for baseline 20 ACAODs of 0 (2a), 0.01 (2b), 0.015 (2c) and 0.02 (2d) respectively, using the CALIOP aerosol layer datasets. Note that different from the cloudy-sky frequency, another way of measuring ACA frequency has been proposed by Devasthale and Thomas (2011) and is referred as the all-sky frequency in this study. The all-sky frequency is defined as number of scenes with ACAOD greater than the baseline resolved over a cloud of 25

## Frequency and Trends of Above-Cloud Aerosols

R. Alfaro-Contreras et al.

Title Page

Abstract

Introduction

Conclusions

References

Tables

Figures



Back

Close

Full Screen / Esc

Printer-friendly Version

Interactive Discussion





COD > 0 divided by the total number of CALIOP scenes per bin. The difference between the two techniques is discussed in more detail during the trend analysis section.

Shown in Fig. 2, no clear difference is observed in the cloudy-sky ACA frequency by applying various CALIOP ACAOD baselines. Similar conclusion can also be made for the June–November period (Fig. 2e–h). Thus, for the purposes of this paper, the baseline CALIOP ACAOD value of 0.015 (0.532  $\mu\text{m}$ ) is chosen, and the sensitivity of ACA trends to the selection of the baseline CALIOP ACAOD is explored in a later section. Additionally, our selection of CALIOP ACAOD baseline has little effect on the background cloudy-sky ACA frequency, which is for the most part, less than 5% (dark blue) throughout the globe. Thus, we arbitrarily select 5% as the threshold between background and significant cloudy-sky ACA frequencies. For the remainder of the paper, ACA frequencies less than five percent are not considered for global distributions of ACA frequencies.

To derive the corresponding noise floor value for above-cloud OMI AI, a pairwise comparison of collocated above-cloud OMI AI and CALIOP AOD has been performed using one year (2007) of collocated OMI-MODIS and CALIOP data as described in Alfaro-Contreras et al. (2014), though without any limitations on the cloud-top height. Figure 3a depicts the relationship between binned above-cloud OMI AI and CALIOP AOD segregated into six different underlying MODIS-derived CODs (Yu et al., 2012; Torres et al., 2012). The bin averaged CALIOP ACAOD of 0.015, the baseline CALIOP ACAOD value chosen above, corresponds to OMI AI values of 0.7–1.2 for underlying MODIS CODs ranging from 0 to 20. Note that, if CALIOP ACAODs are biased low, the corresponding OMI AI thresholds may also bias low using methods as shown in Fig. 3a.

Still, as suggested from Fig. 3a, baseline values of OMI AI vary from 0.7 to 1.2 depending on the underlying cloud properties. To further explore the issue, detected ACA events are evaluated with the use of different baseline OMI AI values, similar to the CALIOP ACAOD baseline analysis and shown in Fig. 3b–i however using only those bin averages with cloudy-sky ACA frequency greater than five percent. Figure 3b–e

Frequency and Trends of Above-Cloud Aerosols

R. Alfaro-Contreras et al.

Title Page	
Abstract	Introduction
Conclusions	References
Tables	Figures
◀	▶
◀	▶
Back	Close
Full Screen / Esc	
Printer-friendly Version	
Interactive Discussion	



## Frequency and Trends of Above-Cloud Aerosols

R. Alfaro-Contreras et al.

Title Page

Abstract

Introduction

Conclusions

References

Tables

Figures

◀

▶

◀

▶

Back

Close

Full Screen / Esc

Printer-friendly Version

Interactive Discussion



depicts the multi-year (2006–2013) cloudy-sky ACA frequency global average for the December–May period, by applying AI baseline thresholds of 0.7 (3b), 0.8 (3c), 0.9 (3d) and 1.0 (3e) respectively. With the use of the baseline OMI AI value of 0.7, most of the remote southern oceans stand out for significant case numbers. By increasing the AI baseline value to 1.0, in contrast, detected ACA events are significantly reduced. A similar conclusion can also be drawn from the June–November period (Fig. 3f–i). Given that hand-held ship borne sun photometer measurements collected by the Marine Aerosol Network (MAN; Smirnov et al., 2011) show an averaged AOD ( $0.55 \mu\text{m}$ ) of 0.07 or less from  $30$  to  $60^\circ \text{S}$  (Toth et al., 2013), significant ACA events are not likely over remote southern oceans. Thus, based on Figs. 2 and 3, CALIOP ACAOD of 0.015 and an above-cloud OMI AI of 1.0 are chosen as baselines.

Selection of baseline above-cloud CALIOP AOD and OMI AI is clearly subjective, and done for qualitative analysis in subsequent sections. There are multiple caveats that must be considered before constraining these values more accurately and representatively. First, as mentioned earlier, the CALIOP instrument has issues in detecting optically thin aerosol layers, especially during daytime. Additionally, it is also reported that CALIOP has a decreased sensitivity to stratospheric aerosols layers (Thomason et al., 2007; Winker et al., 2009). Third, besides aerosol loading, OMI AI is also sensitive to parameters such as aerosol vertical distributions, cloud optical depth of underlying cloud and aerosol single scattering albedo (e.g. Yu et al., 2012). Thus, setting a seasonal and regional based baseline for ACA requires a more in depth analysis and should be considered in future studies. Still, this study presents the first ever attempt to solve ACA baselines and the thresholds selected are the best noise floors we can come up with.

#### 4 Comparison of ACA global climatology using two separate techniques

Figure 4a depicts the multi-year gridded mean near-global distribution ( $180^\circ \text{W}$ – $180^\circ \text{E}$ ,  $45^\circ \text{S}$ – $60^\circ \text{N}$ ) of the OMI-derived daytime cloudy-sky ACA frequency for December to



## Frequency and Trends of Above-Cloud Aerosols

R. Alfaro-Contreras et al.

Title Page

Abstract

Introduction

Conclusions

References

Tables

Figures



Back

Close

Full Screen / Esc

Printer-friendly Version

Interactive Discussion



et al., 2005b), which is detected by both OMI and CALIOP. Therefore, we suspect that their relative differences as derived in Fig. 4i and j are likely linked to the misidentification of thick dust plumes as clouds by the MODIS cloud-masking scheme over the bright desert surfaces (e.g., Levy et al., 2013). Further differences observed between the two datasets may also be due to the different algorithmic sensitivities exhibited to both the optical depth of the underlying cloud and overlying aerosol plume, as well as the OMI AI and CALIOP AOD noise floors used to define the ACA events. We reexamine this point later in the paper.

Compared with daytime, increases in both the spatial extent and cloudy-sky CALIOP ACA frequencies are observable at night, as seen from Fig. 4b, c, e and f over most regions. Over the most common ACA regions, nighttime cloudy-sky ACA frequencies can be 10–30 % higher than during day, which may partially due to the stronger sensitivity of CALIOP at night allowing for detection of optically thin aerosol plumes. In particular, ACA events are observed with extended frequency over the west coast of North America year round and over the west coast of South America for the June–November period. Cloudy-sky ACA frequencies at night, over both of these regions, are composed of optically-thin aerosol loading cases above our defined noise floor. Nighttime ACA events are also observed over the east coast of Asia year round. One reason for differences in spatial coverage between daytime and nighttime ACA events is plausibly linked to a lower planetary boundary layer that affects the formation of low clouds (e.g. Schrage et al., 2012). Still, the discrepancy between nighttime and daytime ACA events can be partially attributed to the potential detection of relatively optically thin above-cloud aerosol plumes that are more detectable during nighttime compared with day as a result of the higher signal to noise ratio for CALIOP nighttime data (e.g. Kacenelenbogen et al., 2014).

Shown in Fig. 5 are averaged above-cloud OMI AI and CALIOP AOD values for corresponding ACA events from Fig. 4. Figure 5a depicts the mean near-global distribution of OMI AI over MODIS-resolved cloudy skies, defined as OMI-MODIS collocated cloudy pixels (cloud fraction of unity) and OMI AI averaged for each  $1^\circ \times 1^\circ$  grid box,

during December to May. Only bins with averaged AI greater than 1.0 are plotted in accordance with our defined noise floor. Figure 5b depicts multi-year mean gridded daytime CALIOP ACAOD averaged for each  $2.5^\circ \times 2.5^\circ$  grid box for CALIOP-defined cloudy pixels (COD > 0), using only bin averaged ACAOD greater than 0.015, also for  
5 December–May. Figure 5c shows the same information as Fig. 5b, now for nighttime CALIOP retrievals.

During the December–May period, elevated OMI AI values are observed over the Saharan desert region of northern Africa, as well as in Southeast Asia off the coast of northern Vietnam. In comparison with OMI AI, CALIOP AOD shows a much broader  
10 distribution of AODs greater than the baseline (ACAOD > 0.015) for the entire globe. Bin averaged AIs greater than the baseline (AI > 1.0) are sparse during the winter and spring months. Additionally, optically thin aerosol plumes are observed over the Northern Pacific and Atlantic Oceans during the CALIOP nighttime analysis (Fig. 5c), when compared to the daytime (Fig. 5b), due to the absence of solar light causing  
15 a decrease in sensitivity in the CALIOP lidar.

Figure 5d–f depicts the same information as Fig. 5a–c, now for the June–November period. This period exhibits a relatively large overall distribution of ACA events. In addition to the Saharan dust outbreaks, elevated AI and AOD values, over the southern Africa smoke region, are also found from both OMI and CALIOP datasets, respectively.  
20 This period exhibits large aerosol loading and ACA frequency over Southern Africa and the southeast Atlantic Ocean. High values of ACAOD are also found over the Indian Ocean and Arabian Sea, due likely to the transport of dust aerosols from the east Saharan and Arabian Gulf regions (Satheesh et al., 2006). Comparing Figs. 4 and 5 over regions such as the west coast of South and North America, it is clear that cloudy-sky ACA frequencies are mostly attributable to relatively low aerosol loading events.  
25 Figure 5 shows a drastically reduced distribution of averaged OMI AIs above the AI baseline (1.0) in comparison to averaged CALIOP ACAODs above the AOD baseline (0.015). This may be as a result of aerosol-free scenes from CALIOP (AOD = 0) be-

## Frequency and Trends of Above-Cloud Aerosols

R. Alfaro-Contreras et al.

Title Page

Abstract

Introduction

Conclusions

References

Tables

Figures

◀

▶

◀

▶

Back

Close

Full Screen / Esc

Printer-friendly Version

Interactive Discussion



ing excluded in the averaging process however all AI values are used in the averaging process, as no such lower boundary exist for defining OMI AI aerosol-free scenes.

Again, differences are visible here between day and night time CALIOP AOD distributions. Off the Southwest coast of Africa, the development of marine stratus-type clouds, as suggested from Fig. 5, may lead to higher ACAOD values at night. Over India and the Middle East, we suspect that higher daytime ACAOD values may exist. Still, lower CALIOP signal-to-noise during daytime may be a limiting factor that contributes significantly to the difference.

It is likely that most ACA events occur over low-level liquid-phase cloud decks. Therefore, spatial distributions of CALIOP-derived low-level clouds are investigated. Figure 6a (6b) depicts the daytime (nighttime) multi-year mean distribution of low-level clouds (defined as the ratio of CALIOP scenes with a COD > 0 and cloud-top height < 3 km over total number of CALIOP scenes) during December 2006–May 2013. CALIOP cloud layer data are gridded into  $2.5^\circ \times 2.5^\circ$  bins. Figure 6c and d depicts the same information as Fig. 6a and b, now from June 2006–November 2013. Figure 6e and f depicts the ratio between daytime and nighttime low-level cloud frequencies per bin for the December–May period and June–November periods, respectively. The ratio is as high as 2.0 over the Northern and Southern Africa regions during June–November, as well as over the Western US annually. Such a high ratio between day and nighttime data leads to a nighttime frequency of 10–20% low-level cloud coverage increase over most regions compared with daytime observations, plausibly due to diurnal boundary layer effects.

A significant percentage of CALIOP-derived low-level clouds are plausibly stratocumulus clouds, which are frequently observed over the west coasts of major continents (e.g. Wood et al., 2012). Qualitative comparison of Figs. 5 and 6 indicates reasonable consistency between high frequencies of CALIOP-defined low-level cloud formation and ACA loading. With the exception of the Saharan region, again due to the possible misclassification of thick aerosol plumes as clouds by MODIS discussed earlier, most ACA loading cases are found where the CALIOP-defined low-level cloud forma-

Frequency and Trends of Above-Cloud Aerosols

R. Alfaro-Contreras et al.

Title Page	
Abstract	Introduction
Conclusions	References
Tables	Figures
◀	▶
◀	▶
Back	Close
Full Screen / Esc	
Printer-friendly Version	
Interactive Discussion	



tion six month frequency exceeds 20 % or more. This indirectly confirms that most ACA outbreaks occur over CALIOP-defined low-level clouds.

It is also useful to evaluate ACA frequency relative to mean clear-sky AOD. Figure 7a–d depicts the multi-year mean clear-sky CALIOP AOD for the same temporal and spatial domains as Fig. 5b, c, e and f, respectively. As opposed to the cloud-sky ACA aerosol loading (Fig. 5), AOD loading over clear-skies shows more activity inland, as the formation of low-level clouds is more common over coastal regions (ICCP, 2007). An inter-comparison among Figs. 5–7 suggests that ACA events do not necessarily follow clear sky AOD patterns but rather those above-cloud aerosol-polluted regions with a high frequency of low-cloud presence.

## 5 Global trend analysis

A global trend analysis of ACA frequency is carried out for five different scenarios. The different scenarios are; OMI daytime cloudy-sky frequency, CALIOP daytime cloudy-sky and all-sky frequencies and CALIOP nighttime cloudy-sky and all-sky frequencies. Figure 8 shows CALIOP daytime cloudy-sky frequency (blue) and all-sky frequency (red), CALIOP nighttime cloudy-sky frequency (purple) and all-sky frequency (orange), and OMI daytime cloudy sky-frequency (green). Each data point represents the global monthly mean ACA frequency of CALIOP and OMI, calculated from 2.5° and 1° gridded ACA frequencies, respectively.

An increase in the OMI cloudy-sky ACA frequency over the study period is apparent in this global dataset, noticeably since 2009. However, this trend is not matched in the CALIOP data. The seasonal variation in ACA frequency is observed from year-to-year for both OMI and CALIOP (dashed lines). However, from the trend lines (showing a percentage change per year), only the OMI daytime cloudy-sky frequency shows a significant increase over this time period (solid lines). The increasing trend in OMI derived daytime global cloudy-sky ACA frequency, not apparent in any of the CALIOP derived trends, is troublesome and may be attributed to any of the different sensitivities

### Frequency and Trends of Above-Cloud Aerosols

R. Alfaro-Contreras et al.

Title Page	
Abstract	Introduction
Conclusions	References
Tables	Figures
◀	▶
◀	▶
Back	Close
Full Screen / Esc	
Printer-friendly Version	
Interactive Discussion	





of the two techniques, including cloud and aerosol optical properties, aerosol-cloud separation distance, and/or deficiencies in the OMI data products. As will be described below, we further investigate several aspects of the observed OMI AI trend.

Given the unexpected monotonic increase in ACA frequency trend derived using OMI AI data, we examine the trend in OMI daytime cloudy-sky ACA frequency more closely. Figure 8a indicates a near-zero increase in the monthly averages during the first few years of the study, with frequencies increasing at a rate of roughly 0.5 % per year starting in 2009. This time period coincides with the start of OMI data loss due to row anomalies, as mentioned above, leading us to further investigate this as a possible reason for the increase in the observed OMI cloudy-sky ACA frequency. Note that we detected data loss while collocating OMI and CALIOP datasets and found no collocated pixels after 2008; a possible sign that the data loss is likely affecting OMI nadir viewing pixels. This is illustrated in Fig. 9a, which depicts a single swath of OMI AI over the African continent on 1 August 2007 where only OMI pixels with valid AI are shown. The data loss affected a large portion of the OMI AI data near the nadir regions of each OMI AI swath, as shown from a swath in 1 June 2009 (Fig. 9b).

Given that the data loss affects mostly nadir-viewing OMI pixels, OMI AI is evaluated as a function of the OMI sensor's viewing zenith angle (VZA) shown in Fig. 10. All OMI AI pixels for one year (2007) are averaged into one-degree VZA bins. Averaged OMI AI values at the edge of the swath are generally higher by about one AI unit than retrievals taken near the center of the swath. Thus, a meaningful trend cannot be established from the OMI data due to the viewing geometry bias impacting later years of the OMI aerosol products. The remainder of the paper will focus solely on trends derived from CALIOP ACA frequencies, and no further discussion of OMI AI frequencies will be carried out.

Next, AERONET AOD data are used to identify a possible bias in the CALIOP lidar due to potential signal deterioration in the instrument. Figure 11 depicts the clear-sky AOD trends derived using collocated CALIOP-AERONET data over all coastal and island AERONET stations (Zhang and Reid, 2006). Trends similar to those for the collo-

## Frequency and Trends of Above-Cloud Aerosols

R. Alfaro-Contreras et al.

Title Page

Abstract

Introduction

Conclusions

References

Tables

Figures



Back

Close

Full Screen / Esc

Printer-friendly Version

Interactive Discussion









cloud aerosol (ACA) events are studied and compared. Active-based profiling is considered an optimal means for identifying ACA occurrence. OMI identification is restricted to ultra-violet (UV)-absorbing ACA events (i.e., smoke), in contrast, through the Aerosol Index (AI) parameter. However, the relatively wide field-of-view of the paired OMI/MODIS datasets, in tandem, provide greater data volume overall, which serves as a relatively well-characterized reference for comparing with CALIOP.

The primary findings of this study are:

1. Baselines values for the passive-based OMI AI as well as active-based CALIOP above-cloud aerosol optical depth (ACAOD) are established in order to distinguish background noise from signal due to significant ACA events such as dust outbreaks and biomass burning. The “baseline” for OMI AI and CALIOP are applied to their respective data sets during processing. However, caution should be exercised when using these baselines, as they are an approximation and will vary depending on ancillary observational parameters for OMI and day vs. nighttime sensitivity for CALIOP.
2. Despite fundamental differences in spatial and vertical samplings, as well as sensitivity to ACA aerosol types, both OMI- and CALIOP-based techniques broadly resolve consistent global/spatial distributions of cloudy-sky ACA frequency. For example, both capture ACA events over the Northwest Coast of Africa and the Arabian Peninsula during the December–May period, and over the North- and South-west Coast, as well as the Southeast Coast of Africa, the Arabian Peninsula and Arabian Sea during the June–November period. Still, discrepancies, as expected, are present. For example, daytime cloudy-sky ACA frequencies of up to 10 % are found from CALIOP over Southeast Asia during the June–November period. Such ACA events are none existent using OMI-based method, however we are not certain of the reason for the discrepancy over this region. Over North Africa, cloudy-sky ACA frequencies of around 20 % are reported for both periods from the OMI-based method, yet such events are largely undetected by the

Frequency and Trends of Above-Cloud Aerosols

R. Alfaro-Contreras et al.

Title Page

Abstract

Introduction

Conclusions

References

Tables

Figures



Back

Close

Full Screen / Esc

Printer-friendly Version

Interactive Discussion



## Frequency and Trends of Above-Cloud Aerosols

R. Alfaro-Contreras et al.

Title Page

Abstract

Introduction

Conclusions

References

Tables

Figures



Back

Close

Full Screen / Esc

Printer-friendly Version

Interactive Discussion



CALIOP-based method. We suspect that heavy dust plumes may be misidentified as clouds by the passive-based method, thus causing an unexpected rise in the passive-based derived cloudy-sky ACA frequency over that region.

3. CALIOP nighttime data exhibit slightly larger distributions and a 10–20 % greater cloudy-sky ACA frequency annually in comparison to daytime. This may be due the lowering of the planetary boundary layer at night, influencing frequencies of low-cloud formation, as well as the impact of higher signal-to-noise in nighttime CALIOP datasets for subsequent Level 2 analysis partly controlled for in our study by applying the noise floor. To the latter point, previous study has shown relative stability between day/night CALIOP aerosol products (Campbell et al., 2012). However, the implicit effect on the vertical distribution of aerosol occurrence was not specifically investigated. More detailed study is needed to reconcile this finding.
4. A global trend analysis shows a near-zero negligible slope in the global CALIOP cloudy-sky and all-sky ACA frequencies. However, OMI-MODIS cloudy-sky daytime ACA frequencies show an increase of  $\sim 0.5\% \text{ year}^{-1}$  since 2009 possibly due to a significant loss in the OMI data starting in 2009, mostly for nadir viewing pixels. Investigation of the relationship between OMI Aerosol Index (AI) and satellite viewing zenith angle, suggests a viewing angle dependency of OMI AI. Considering that OMI AI increases near the edge of the viewing swath, it is possible that the overall increase in ACA frequency is due to the significant loss of OMI AI data during later years of the study.
5. A decrease in the cloudy-sky global ACA frequency and data counts ranging from 1–2 % and 1–3 million, respectively, as a result of applying a variety of thresholds to the ACAOD and/or underlying cloud optical depth (COD) during sensitivity analysis. COD thresholds of 0.3 and 2.5 filter high cirrus clouds and non-contiguous low-level water clouds, respectively. Additionally, CALIOP data are reprocessed with no restriction to the ACAOD. Most threshold tests show a reduction in global

## Frequency and Trends of Above-Cloud Aerosols

R. Alfaro-Contreras et al.

Title Page

Abstract

Introduction

Conclusions

References

Tables

Figures



Back

Close

Full Screen / Esc

Printer-friendly Version

Interactive Discussion



ACA frequencies however those ACA events located over optically thick clouds (COD > 2.5) show a near zero trend. However, a significant change to CALIOP global day or nighttime ACA frequency trends is not apparent.

- 5 6. Globally, clear-sky AOD trends are slightly positive while cloudy-sky ACA frequency exhibits a positive trend in the day and negative during night while the opposite is true for ACAOD trends. Some select regions examined globally, selected for their relatively high ACA frequency overall, exhibit a consistent trend in all three parameters. Other regions exhibit agreement between some, but not all, parameters. However, neither the regional or global trends of any of the three parameters are statistically significant. An ACA data record spanning at least 30 years is needed in order to report a 10 % per decade change in ACA frequency with 95 % confidence.

15 This study confirms that ACA events occur with a frequency of 1–5 % globally and as high as 14 % over some of the most ACA abundant regions. The two complementary techniques applied to locate ACA events and derive global and regional distributions and long-term trends both exhibit strengths and weaknesses. This study shows that, when used simultaneously, combined passive/active analysis can help present a more comprehensive analysis of ACA than a single-sensor analysis alone. However, the analysis strongly reinforces the use of active-based lidar profiling for distinguishing aerosol presence that perturbs passive-based column-integrated radiative parameters. The vertical distribution and optical properties of aerosol and cloud layers are fundamental to accurate column radiative closure. The effects cloud-aerosol overlap can exhibit on cloud and aerosol property retrieval techniques demands some coordinated active/passive observation for ensuring clarity and limiting bias in top-of-atmosphere retrievals.

25 Due to the extensive spatial coverage and consistency of retrieved datasets from space-borne instruments, trend analyses, and the need for consistent multi-sensor profiling, should become primary motivating factors behind mission design and life ex-



**Frequency and  
Trends of  
Above-Cloud  
Aerosols**

R. Alfaro-Contreras et al.

[Title Page](#)[Abstract](#)[Introduction](#)[Conclusions](#)[References](#)[Tables](#)[Figures](#)[◀](#)[▶](#)[◀](#)[▶](#)[Back](#)[Close](#)[Full Screen / Esc](#)[Printer-friendly Version](#)[Interactive Discussion](#)

pectancy in orbit. Our analysis shows that in a few decades, proper analysis of ACA trends are possible through continuation of a CALIOP/OMI-like paradigm. Ultimately, this work, paired with Alfaro-Contreras (2014) and others, have broadly conceptualized the ACA problem globally. However, the question now turns to whether or not ACA represents a fundamental climate phenomenon that requires specific monitoring long-term in a potentially-changing climate. Trend analysis, then, will help ultimately distinguish this attribute, and thus whether or not ACA is simply noise or a radiatively-significant process that is sensitive to changes in land-use globally and a fluctuating frequency and distribution of elevated aerosol particles over time. Future satellite mission designs should emphasize extending the life of these instruments for application to environmental parameter trend studies.

*Acknowledgements.* This research is funded through the support of the Office of Naval Research Codes 322. Author J. R. Campbell acknowledges the support of the NASA Interagency Agreement IAARPO201422 on behalf of the CALIPSO Science Team. We thank the AERONET program and their contributing principal investigators for collecting and maintaining the sun-photometer data. CALIOP cloud and aerosol layer data were obtained from the Atmospheric Science Data Center. MODIS cloud data were obtained from the Goddard Space Flight Center Level 1 and atmospheric archive and distribution center system. The OMI aerosol data were obtained from the Goddard Earth Science Data Center and Information Service Center.

## References

- Ackerman, S. A., Strabala, K. I., Menzel, W. P., Frey, R. A., Moeller, C. C., and Gumley, L. E.: Discriminating clear sky from clouds with MODIS, *J. Geophys. Res.*, 103, 32141–32157, doi:10.1029/1998JD200032, 1998.
- Ackerman, S. A., Holz, R. E., Frey, R., Eloranta, E. W., Maddux, B., and McGill, M. J.: Cloud detection with MODIS: Part II. Validation, *J. Atmos. Ocean. Tech.*, 25, 1073–1086, 2008.
- Ackerman, S. A., Frey, R., Strabala, K., Liu, Y., Gumley, L., Baum, B., and Menzel, P.: Discriminating clear-sky from cloud with MODIS algorithm theoretical basis document (MOD35), ATBD Reference Number: ATBD-MOD-06, 2010.

## Frequency and Trends of Above-Cloud Aerosols

R. Alfaro-Contreras et al.

Title Page

Abstract

Introduction

Conclusions

References

Tables

Figures



Back

Close

Full Screen / Esc

Printer-friendly Version

Interactive Discussion



Alfaro-Contreras, R., Zhang, J., Reid, J. S., Campbell, J. R., and Holz, R. E.: Evaluating the impact of aerosol particles above cloud on cloud optical depth retrievals from MODIS, *J. Geophys. Res. Atmos.*, 119, 5410–5423, doi:10.1002/2013JD021270, 2014.

Brioude, J., Cooper, O. R., Feingold, G., Trainer, M., Freitas, S. R., Kowal, D., Ayers, J.K., Prins, E., Minnis, P., McKeen, S. A., Frost, G. J., and Hsie, E.-Y.: Effect of biomass burning on marine stratocumulus clouds off the California coast, *Atmos. Chem. Phys.*, 9, 8841–8856, doi:10.5194/acp-9-8841-2009, 2009.

Campbell, J. R., Tackett, J. L., Reid, J. S., Zhang, J., Curtis, C. A., Hyer, E. J., Sessions, W. R., Westphal, D. L., Prospero, J. M., Welton, E. J., Omar, A. H., Vaughan, M. A., and Winker, D. M.: Evaluating nighttime CALIOP 0.532  $\mu\text{m}$  aerosol optical depth and extinction coefficient retrievals, *Atmos. Meas. Tech.*, 5, 2143–2160, doi:10.5194/amt-5-2143-2012, 2012.

Campbell, J. R., Vaughan, M. A., Oo, M., Holz, R. E., Lewis, J. R., and Welton, E. J.: Distinguishing cirrus cloud presence in autonomous lidar measurements, *Atmos. Meas. Tech.*, 8, 435–449, doi:10.5194/amt-8-435-2015, 2015.

Chand, D., Anderson, T. L., Wood, R., Charlson, R. J., Hu, Y., Liu, Z., and Vaughn, M.: Quantifying above-cloud aerosol using space borne lidar for improved understanding of cloudy sky direct climate forcing, *J. Geophys. Res.*, 113, D12306, doi:10.1029/2007JD009443, 2008.

Chand, D., Wood, R., Anderson, T. L., Satheesh, S. K., and Charlson, R. J.: Satellite-derived direct radiative effect of aerosols dependent on cloud cover, *Nat. Geosci.*, 2, 181–184, doi:10.1038/NGEO437, 2009.

Coddington, O. M., Plewskie, P., Redemann, J., Platnick, S., Russell, P. B., Schmidt, K. S., Gore, W. J., Livingston, J., Wind, G., and Vukicevic, T.: Examining the impact of overlying aerosols on the retrieval of cloud optical properties from passive remote sensing, *J. Geophys. Res.*, 115, D10211, doi:10.1029/2009JD012829, 2010.

Devasthale, A. and Thomas, M. A.: A global survey of aerosol-liquid water cloud overlap based on four years of CALIPSO-CALIOP data, *Atmos. Chem. Phys.*, 11, 1143–1154, doi:10.5194/acp-11-1143-2011, 2011.

Eck, T. F., Holben, B. N., Reid, J. S., Dubovik, O., Smirnov, A., O'Neill, N. T., Slutsker, I., and Kinne, S.: Wavelength dependence of the optical depth of biomass burning, urban and desert dust aerosols, *J. Geophys. Res.*, 104, 31333–31349, doi:10.1029/1999JD90093, 1999.

## Frequency and Trends of Above-Cloud Aerosols

R. Alfaro-Contreras et al.

Title Page

Abstract

Introduction

Conclusions

References

Tables

Figures



Back

Close

Full Screen / Esc

Printer-friendly Version

Interactive Discussion



Haywood, J. M., Osborne, S. R., and Abel, S. J.: The effect of overlying absorbing aerosol layers on remote sensing retrievals of cloud effective radius and cloud optical depth, *Q. J. R. Meteorol. Soc.*, 130, 779–800, doi:10.1256/qj.03.100., 2004.

Holben, B. N., Eck, T. F., Slutsker, I., Tanre, D., Buis, J. P., Setzer, A., Vermote, E., Reagan, J. A., Kaufman, Y. J., Nakajima, T., Lavenu, F., Jankowiak, I., and Smirnov, A.: AERONET – a federated instrument network and data archive for aerosol characterization, *Remote Sens. Environ.*, 66, 1–16, 1998.

Holz, R. E., Ackerman, S. A., Nagle, F. W., Frey, R., Dutcher, S., Kuehn, R. E., Vaughn, M. A., and Baum, B.: Global Moderate Resolution Imaging and Spectroradiometer (MODIS) cloud detection and height evaluation using CALIOP, *J. Geophys. Res.*, 113, D00A19, doi:10.1029/2008JD009837, 2008.

Hsu, N. C., Gautam, R., Sayer, A. M., Bettenhausen, C., Li, C., Jeong, M. J., Tsay, S.-C., and Holben, B. N.: Global and regional trends of aerosol optical depth over land and ocean using SeaWiFS measurements from 1997 to 2010, *Atmos. Chem. Phys.*, 12, 8037–8053, doi:10.5194/acp-12-8037-2012, 2012.

Intergovernmental Panel on Climate Change (IPCC): The physical science basis, and contribution of working group I to the fourth assessment report of the IPCC 916, Cambridge Univ. Press, Cambridge, 2007.

Kacenelebogen, M., Redemann, J., Vaughan, M. A., Omar, A. H., Russell, P. B., Burton, S., Rogers, R. R., Ferrare, R. A., and Hostetler, C. A.: An evaluation of CALIOP/CALIPSO's aerosol-above-cloud detection and retrieval capability over North America, *J. Geophys. Res. Atmos.*, 119, 230–244, doi:10.1002/2013JD020178, 2014.

Kahn, R. A., Garay, M. J., Nelson, D. L., Levy, R. C., Bull, M. A., Diner, D. J., Martonchik, J. V., Hansen, E. G., Remer, L. A., and Tanre, D.: Response to “Toward unified satellite climatology and aerosol properties. 3. MODIS versus MISR AERONET”, *J. Quant. Spectrosc. Ra.*, 112, 901–909, doi:10.1016/j.jqsrt.2010.11.001, 2011.

Kaufman, Y. J., Remer, L. A., Tanre, D., Li, R. R., Kleidman, R., Mattoo, S., Levy, R., Eck, T., Holben, B. N., Ichoku, C., Martins, J., and Koren, I.: A critical examination of the residual cloud contamination and diurnal sampling effects on MODIS estimates of the aerosol over ocean, *IEEE T. Geosci. Remote*, 43, 2886–2897, 2005a.

Kaufman, Y. J., Koren, I., Remer, L. A., Tanre, D., Ginoux, P., and Fan, S.: Dust transport and deposition observed from the Terra-Moderate Resolution Imaging Spectro-

**Frequency and  
Trends of  
Above-Cloud  
Aerosols**

R. Alfaro-Contreras et al.

[Title Page](#)[Abstract](#)[Introduction](#)[Conclusions](#)[References](#)[Tables](#)[Figures](#)[◀](#)[▶](#)[◀](#)[▶](#)[Back](#)[Close](#)[Full Screen / Esc](#)[Printer-friendly Version](#)[Interactive Discussion](#)

diometer (MODIS) spacecraft over the Atlantic Ocean, *J. Geophys. Res.*, 110, D10S12, doi:10.1029/2003JD004436, 2005b.

King, M. D., Tsay, S. C., Platnick, S. E., Menghua, W., and Liou, K. N.: Cloud retrievals algorithm for MODIS: optical thickness, effective particle radius and thermodynamic phase, Algorithm Theor. Basis Doc. ATBD-MOD-05, NASA Goddard Space Flight Cent., Greenbelt, MD, 1997.

Leahy, L. V., Wood, R., Charlson, R. J., Hostetler, C. A., Rogers, R. R., Vaughan, M. A., and Winker, D. M.: On the nature and extent of optically thin marine low clouds, *J. Geophys. Res.*, 117, D22201, doi:10.1029/2012JD017929, 2012.

Levy, R. C., Mattoo, S., Munchak, L. A., Remer, L. A., Sayer, A. M., Patadia, F., and Hsu, N. C.: The Collection 6 MODIS aerosol products over land and ocean, *Atmos. Meas. Tech.*, 6, 2989–3034, doi:10.5194/amt-6-2989-2013, 2013.

Li, Z., Zhao, F., Liu, J., Jiang, M., Zhao, C., and Cribb, M.: Opposite effects of absorbing aerosols on the retrievals of cloud optical depth from spaceborne and ground-based measurements, *J. Geophys. Res.-Atmos.*, 119, 5104–5114, doi:10.1002/2013JD021053, 2014.

Liu, Z., Winker, D. M., Omar, A. H., Vaughan, M. A., Kar, J., Trepte, C. R., and Hu, Y.: Evaluation of CALIOP 532-nm AOD over clouds, AGU Fall Meeting 2013, 2013.

Meyer, K., Platnick, S., Oreopoulos, L., and Lee, D.: Estimating the direct radiative effect of absorbing aerosols overlying marine boundary layer clouds in the southeast Atlantic using MODIS and CALIOP, *J. Geophys. Res. Atmos.*, 118, 4801–4815, doi:10.1002/jgrd.50449, 2013.

Peters, K., Quaas, J., and Bellouin, N.: Effects of absorbing aerosols in cloudy skies: a satellite study over the Atlantic Ocean, *Atmos. Chem. Phys.*, 11, 1393–1404, doi:10.5194/acp-11-1393-2011, 2011.

Platnick, S., Pincus, R., Wind, B., King, M. D., Gray, M. A., and Hubanks, P.: An initial analysis of the pixel-level uncertainties in the global MODIS cloud optical thickness and effective particle radius size retrievals, *Proc. SPIE 5652, Passive Optical Remote Sensing of the Atmosphere and Cloud IV*, 30, doi:10.1117/12.578353, 2004.

Powell., K. A., Hostetler, C. A., Liu, Z., Vaughan, M. A., Kuehn, R. E., Hunt, W. H., Lee, K. M., Trepte, C. R., Rogers, R. R., Young, S. A., and Winker, D. M.: CALIPSO lidar calibration algorithms, part I: Nighttime 532-nm-parallel channel 532-nm perpendicular channel, *J. Atmos. Ocean. Tech.*, 26, 2015–2033, 2009.

## Frequency and Trends of Above-Cloud Aerosols

R. Alfaro-Contreras et al.

Title Page

Abstract

Introduction

Conclusions

References

Tables

Figures

◀

▶

◀

▶

Back

Close

Full Screen / Esc

Printer-friendly Version

Interactive Discussion



Remer, L. A., Kaufman, Y. J., Tanre, D., Mattoo, S., Chu, D. A., Martins, J. V., Li, R. R., Ichoku, C., Levy, R. C., Kleidman, R. G., Eck, T. F., Vermote, E., and Holben, B. N.: The MODIS aerosol algorithm, products and validation. *J. Atmos. Sci.*, 62, 947–973, 2005.

Remer, L. A., Kleidman, R. G., Levy, R. C., Kaufman, Y. J., Tanre, D., Mattoo, S., Martins, J. V., Ichoku, C., Koren, I., Yu, H., and Holben, B. N.: Global aerosol climatology from MODIS satellite sensors, *J. Geophys. Res.*, 113, D14S07, doi:10.1029/2007JD009661, 2008.

Roberts, G., Wooster, M. J., and Lagoudakis, E.: Annual and diurnal african biomass burning temporal dynamics, *Biogeosciences*, 6, 849–866, doi:10.5194/bg-6-849-2009, 2009.

Rossow, W. B. and Schiffer, R. A.: Advances in understanding clouds from ISCCP, *B. Am. Meteorol. Soc.*, 80, 2261–2287, doi:10.1175/1520-04771999:080<2261:AIUCFI>2.0.CO;2, 1999.

Royal Netherlands Meteorological Society: Background information about Row Anomaly in OMI, available at: [www.knmi.nl/omi/research/product/rowanomaly-background.php](http://www.knmi.nl/omi/research/product/rowanomaly-background.php), accessed on December 22 2014

Sassen, K. and Cho, B. S.: Subvisual-thin cirrus lidar dataset for satellite verification and climatological research, *J. Appl. Meteorol.*, 31, 1275–1285, 1992.

Satheesh, S. K., Morthy, K. K., Kaufman, Y. J., and Takemura, T.: Aerosol optical depth, physical properties and radiative forcing over the Arabian Sea, *Meteorol. Atmos. Phys.*, 91, 45–62, 2006.

Sayer, A. M., Hsu, N. C., Bettenhausen, C., Ahmad, Z., Holben, B. N., Smirnov, A., Thomas, G. E., and Zhang, J.: SeaWiFS Ocean Aerosol Retrievals (SOAR): algorithm, validation, and comparison with other datasets, *J. Geophys. Res.*, 117, D03206, doi:10.1029/2011JD016599, 2012.

Schrage, J. M. and Fink, A. H.: Nocturnal continental low-level stratus over Tropical West Africa: observations and possible mechanisms controlling its onset, *Mon. Weather Rev.*, 140, 1794–1809, doi:10.1175/MWR-D-11-00172.1, 2012.

Shi, Y., Zhang, J., Reid, J. S., Holben, B., Hyer, E. J., and Curtis, C.: An analysis of the collection 5 MODIS over-ocean aerosol optical depth product for its implication in aerosol assimilation, *Atmos. Chem. Phys.*, 11, 557–565, doi:10.5194/acp-11-557-2011, 2011.

Smirnov, A., Holben, B. N., Giles, D. M., Slutsker, I., O'Neill, N. T., Eck, T. F., Macke, A., Croot, P., Courcoux, Y., Sakerin, S. M., Smyth, T. J., Zielinski, T., Zibordi, G., Goes, J. I., Harvey, M. J., Quinn, P. K., Nelson, N. B., Radionov, V. F., Duarte, C. M., Losno, R., Sciare, J., Voss, K. J., Kinne, S., Nalli, N. R., Joseph, E., Krishna Moorthy, K., Covert, D. S.,

## Frequency and Trends of Above-Cloud Aerosols

R. Alfaro-Contreras et al.

Title Page

Abstract

Introduction

Conclusions

References

Tables

Figures

◀

▶

◀

▶

Back

Close

Full Screen / Esc

Printer-friendly Version

Interactive Discussion

Gulev, S. K., Milinevsky, G., Larouche, P., Belanger, S., Horne, E., Chin, M., Remer, L. A., Kahn, R. A., Reid, J. S., Schulz, M., Heald, C. L., Zhang, J., Lapina, K., Kleidman, R. G., Griesfeller, J., Gaitley, B. J., Tan, Q., and Diehl, T. L.: Maritime aerosol network as a component of AERONET – first results and comparison with global aerosol models and satellite retrievals, *Atmos. Meas. Tech.*, 4, 583–597, doi:10.5194/amt-4-583-2011, 2011.

Stephens, G. L., Vane, D. G., Boain, R. J., Mace, G. G., Sassen, K., Wang, Z., Illingsworth, A. J., O'Connor, E. J., Rossow, W. B., Durden, S. L., Miller, S. D., Austin, R. T., Benedetti, A., and Mitrescu, C.: The Cloudsat mission and the A-Train, *B. Am. Meteorol. Soc.*, 83, 1771–1790, doi:10.1175/BAMS-83-12-1771, 2002.

Stevens, B. and Fetingold, G.: Untangling aerosol effects on clouds and precipitation in a buffered system, *Nature*, 461, 607–613, 2009.

Thomason, L. W., Pitts, M. C., and Winker, D. M.: CALIPSO observations of stratospheric aerosols: a preliminary assessment, *Atmos. Chem. Phys.*, 7, 5283–5290, doi:10.5194/acp-7-5283-2007, 2007.

Torres, O., Bhartia, P. K., Herman, J. R., and Ahmad, Z.: Derivation of aerosol properties from satellite measurements of backscattered ultraviolet radiation: theoretical basis, *J. Geophys. Res.*, 103, 17110, doi:10.1029/98JD00900, 1998.

Torres, O., Tanskanen, A., Viehmann, B., Ahn, C., Braak, R., Bhartia, P. K., Veefkind, P., and Levelt, P.: Aerosols and surface UV products from Ozone Monitoring observations: an overview, *J. Geophys. Res.*, 112, D24S47, doi:10.1029/2007JD008809, 2007.

Torres, O., Jethva, H., and Bhartia, P. K.: Retrieval of aerosol optical depth above clouds from OMI observations: sensitivity analysis and case studies. *J. Atmos. Sci.*, 69, 1037–1053, 2012.

Waquet, F., Reidi, J., Labonnote, L. C., Goloub, P., Cairns, B., Deuze, J. L., and Tanre, D.: Aerosol remote sensing over clouds using A-train observations, *J. Atmos. Sci.*, 66, 2468–2480, 2009.

Weatherhead, E. C., Reinsel, G. C., Tiao, G. C., Meng, X. L., Choi, D., Cheang, W. K., Keller, T., DeLuisi, J., Wuebbles, D. J., Kerr, J. B., Miller, A. J., Oltmans, S. J., and Frederick, J. E.: Factors affecting the detection of trends: statistical considerations and applications to environmental data, *J. Geophys. Res.*, 103, 17149–17161, 1998.

Wetherald, R. T. and Manabe, S.: Cloud feedback processes in a general circulation model *J. Atmos. Sci.*, 45, 1397–1415, 1988.

## Frequency and Trends of Above-Cloud Aerosols

R. Alfaro-Contreras et al.

Title Page

Abstract

Introduction

Conclusions

References

Tables

Figures



Back

Close

Full Screen / Esc

Printer-friendly Version

Interactive Discussion



- Wilcox, E. M.: Direct and semi-direct radiative forcing of smoke aerosols over clouds, *Atmos. Chem. Phys.*, 12, 139–149, doi:10.5194/acp-12-139-2012, 2012.
- Wilcox, E. M., Harshvardian and Platnick, S.: Estimate of the impact of absorbing aerosol over cloud on the MODIS retrievals of cloud optical thickness and effective radius using two independent retrievals of liquid water path, *J. Geophys. Res.*, 114, D05210, doi:10.1029/2008JD010589, 2009.
- Winker, D. M., Vaughan, M. A., Omar, A. H., Hu, Y., Powell, K. A., Liu, Z., Hunt, W. H., and Young, S. A.: Overview of the CALIPSO mission and CALIOP data processing Algorithm. *J. Atmos. Ocean. Tech.*, 26, 2310–2323, doi:10.1175/2009TECHA.1281.1, 2009.
- Winker, D. M. and coauthors.: The CALIPSO mission: a global 3D view of aerosols and clouds, *B. Am. Meteorol. Soc.*, 91, 1211–1229, 2010.
- Wood, R.: Stratocumulus clouds, *Mon. Weather Rev.*, 140, 2373–2423, 2012.
- Yu, H., Dickinson, R., Chin, M., Kaufman, Y., Holben, B., Geogdzhayev, I., and Mishchenko, M.: Annual cycle of global distributions of aerosol optical depth from integration of MODIS retrievals and GOCART model simulations, *J. Geophys. Res.*, 108, 4128, doi:10.1029/2002JD002717, 2003.
- Yu, H., Zhang, Y., Chin, H., Liu, Z., Omar, A., Remer, L. A., Yang, Y., Yuan, T., and Zhang, J.: An integrated analysis of aerosols above-clouds from A-train multi sensor measurements, *Remote Sens. Environ.*, 121, 125–131, 2012.
- Zhang, J. and Reid, J. S.: MODIS aerosol product analysis for data assimilation: assessment of level 2 aerosol optical thickness retrievals, *J. Geophys. Res.*, 111, D222077, doi:10.1029/2005JD006898, 2006.
- Zhang, J. and Reid, J. S.: A decadal regional and global trend analysis of the aerosol optical depth using a data-assimilation grade over-water MODIS and Level 2 MISR aerosol products, *Atmos. Chem. Phys.*, 10, 10949–10963, doi:10.5194/acp-10-10949-2010, 2010.
- Zhang, J., Christopher, S. A., and Holben, B. N.: Intercomparison of smoke aerosol optical thickness derived from GOES 8 imager and ground-based Sun photometers, *J. Geophys. Res.*, 106, 7387–7397, doi:10.1029/2000JD900540, 2001.
- Zhang, J., Campbell, J. R., Reid, J. S., Westphal, D. L., Baker, N. L., Campbell, W. F., and Hyer, E. J.: Evaluating the impact of assimilating CALIOP-derived aerosol extinction profiles on a global mass transport model, *Geophys. Res. Lett.*, 38, L14801, doi:10.1029/2011GL047737, 2011.



Zhang, J., Reid, J. S., Campbell, J. R., Hyer, E. J., and Westphal, D. L.: Evaluating the impact of multi-sensor data assimilation on a global aerosol particle transport model, *J. Geophys. Res. Atmos.*, 119, 4674–4689, doi:10.1002/2013JD020975, 2014.

5 Zhang, Z., Meyer, K., Platnick, S., Oreopoulos, L., Lee, D., and Yu, H.: A novel method for estimating shortwave direct radiative effect of above-cloud aerosols using CALIOP and MODIS data, *Atmos. Meas. Tech.*, 7, 1777–1789, doi:10.5194/amt-7-1777-2014, 2014.

## ACPD

15, 4173–4217, 2015

### Frequency and Trends of Above-Cloud Aerosols

R. Alfaro-Contreras et al.

Title Page

Abstract

Introduction

Conclusions

References

Tables

Figures



Back

Close

Full Screen / Esc

Printer-friendly Version

Interactive Discussion



## Frequency and Trends of Above-Cloud Aerosols

R. Alfaro-Contreras et al.

**Table 1.** Global cloudy-sky relative frequency and data counts for the sensitivity test carried out in Section 6. A total of five different threshold tests are applied to both day and nighttime CALIOP cloud and aerosol layer products.

	Day	Night
Total Cloudy Scenes	103 977 800/	94 461 656/
(Column COD > 0/0.3/2.5)	79 513 688/	73 606 408/
	45 003 964	42 543 896
Data counts/Mean global ACA relative frequency		
COD > 0 and AOD > 0	2 074 636/2.0 %	4 165 264/4.41 %
COD > 0.3 and AOD > 0	1 030 343/1.29 %	3 188 653/4.33 %
COD > 2.5 and AOD > 0	651 730/1.44 %	2 324 228/5.46 %
COD > 0.3 and AOD > 0.015	808 567/1.02 %	1 744 929/2.37 %
COD > 2.5 and AOD > 0.015	498 070/1.11 %	1 280 004/3.0 %
COD > 0 and AOD > 0.015	1 690 221/1.63 %	2 331 364/2.47 %

Title Page

Abstract

Introduction

Conclusions

References

Tables

Figures



Back

Close

Full Screen / Esc

Printer-friendly Version

Interactive Discussion



## Frequency and Trends of Above-Cloud Aerosols

R. Alfaro-Contreras et al.

Title Page

Abstract

Introduction

Conclusions

References

Tables

Figures

◀

▶

◀

▶

Back

Close

Full Screen / Esc

Printer-friendly Version

Interactive Discussion



**Table 2.** Seven and a half year above-cloud aerosol cloudy-sky frequency, AOD and clear-sky AOD yearly trend analysis for the selected target regions. All underlying cloud layers are considered in this analysis. Trend analysis for the entire globe is also included. For each region, three parameters, the ACA cloudy-sky frequency, above-cloud aerosol AOD and clear-sky AOD values are reported. Note that the clear sky AOD trends are estimated using 100 % cloud free data from the CALIOP cloud and aerosol layer products.

Region	Latitude (°)	Longitude (°)	Slope/per year (CALIOP day-time) (%)	Trend significance CALIOP day-time ( $\omega/\sigma\omega$ )	Slope/per year (CALIOP night-time) (%)	Trend Significance CALIOP night-time ( $\omega/\sigma\omega$ )
ACA cloudy-sky frequency (%) / Above-cloud aerosol AOD / clear-sky AOD						
Southern Africa	37° S–5° N	30° W–30° E	~ 0/ -0.002/ -0.0004	~0/ 0.231/ 0.04	0.19/ 0.001/ 0.001	0.19/ 0.062/ 0.08
Northern Africa	5–35° N	70° W–25° E	0.006/ -0.003/ -0.001	0.008/ 0.210/ 0.07	0.053/ -0.001/ -0.002	0.089/ 0.056/ 0.09
Southeast Asia	10–25° N	90–150° E	-0.248/ 0.001/ -0.002	0.0311/ 0.09/ 0.1	-0.009/ -0.002/ -0.0004	0.015/ 0.094/ 0.02
China	30–55° N	110–160° E	-0.092/ 0.0001/ 0.001	0.159/ 0.020/ 0.01	-0.081/ -0.001/ 0.0002	0.062/ 0.119/ 0.01
Middle East	10–40° N	30–55° E	0.407/ 0.002/ 0.006	0.168/ 0.070/ 0.16	0.452/ 0.003/ 0.005	0.264/ 0.083/ 0.13
South America	20° S–10° N	105–60° W	-0.082/ -0.0003/ -0.002	0.129/ 0.027/ 0.12	-0.150/ -0.002/ -0.002	0.098/ 0.175/ 0.09
India	0–30° N	60–85° E	0.319/ ~0/ 0.008	0.194/ 0.001/ 0.20	0.105/ 0.002/ 0.01	0.095/ 0.040/ 0.19
North America	20–60° N	160–110° W	-0.043/ 0.0002/ ~ 0	0.069/ 0.029/ 0.003	-0.064/ -0.0005/ -0.0003	0.037/ 0.094/ 0.04
Southern Oceans	40–12° S	35–115° E	-0.013/ 0.001/ 0.001	0.033/ 0.130/ 0.29	0.066/ -0.001/ 0.0008	0.050/ 0.160/ 0.21
Global			0.007/ -0.0001/ 0.0005	0.042/ 0.050/ 0.13	-0.008/ 0.0003/ 0.0007	0.020/ 0.105/ 0.18

## Frequency and Trends of Above-Cloud Aerosols

R. Alfaro-Contreras et al.

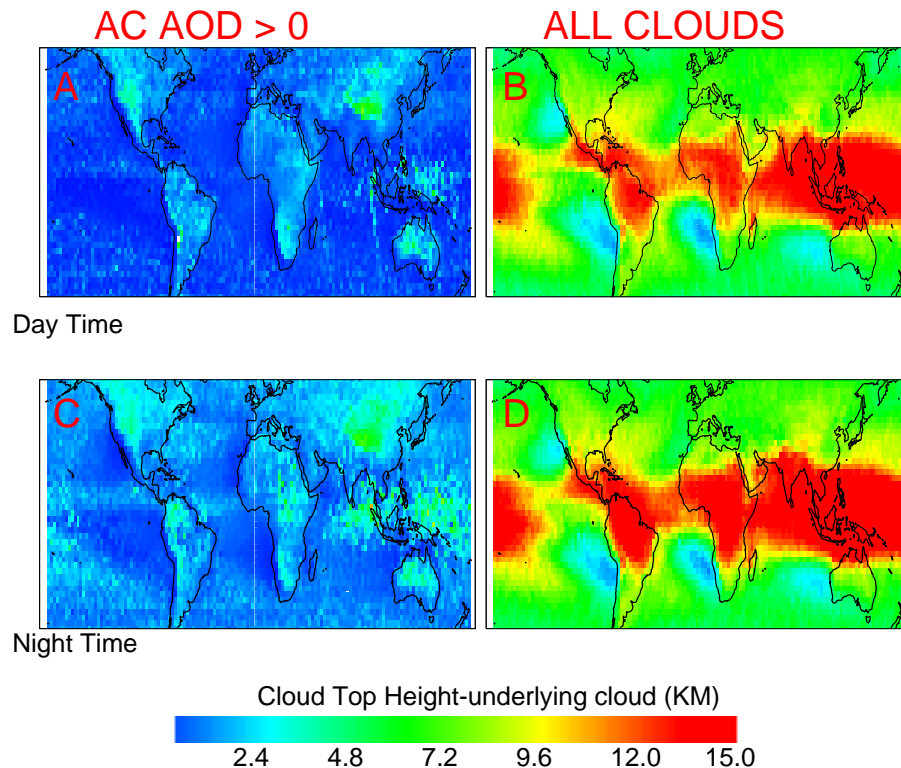


**Figure 1.** (a) Multi-year (June 2006–November 2013) cloud-top heights (above sea level) of the underlying cloud in the ACA scenarios averaged into  $2.5^\circ \times 2.5^\circ$  bins derived from CALIOP cloud and aerosol layer data sets for the entire year for the daytime observations. Only those clouds with a retrieved aerosol plume (ACAOD > 0) overhead are used in the averaging process for CALIOP daytime observations. (b). Cloud-top heights averaged similar to Fig. 1a however using all CALIOP scenes with column COD > 0 regardless of the AOD. (c and d) show the same information as Figs. 1a and b during nighttime observations.

Title Page

Abstract

Introduction

Conclusions

References

Tables

Figures

◀

▶

◀

▶

Back

Close

Full Screen / Esc

Printer-friendly Version

Interactive Discussion

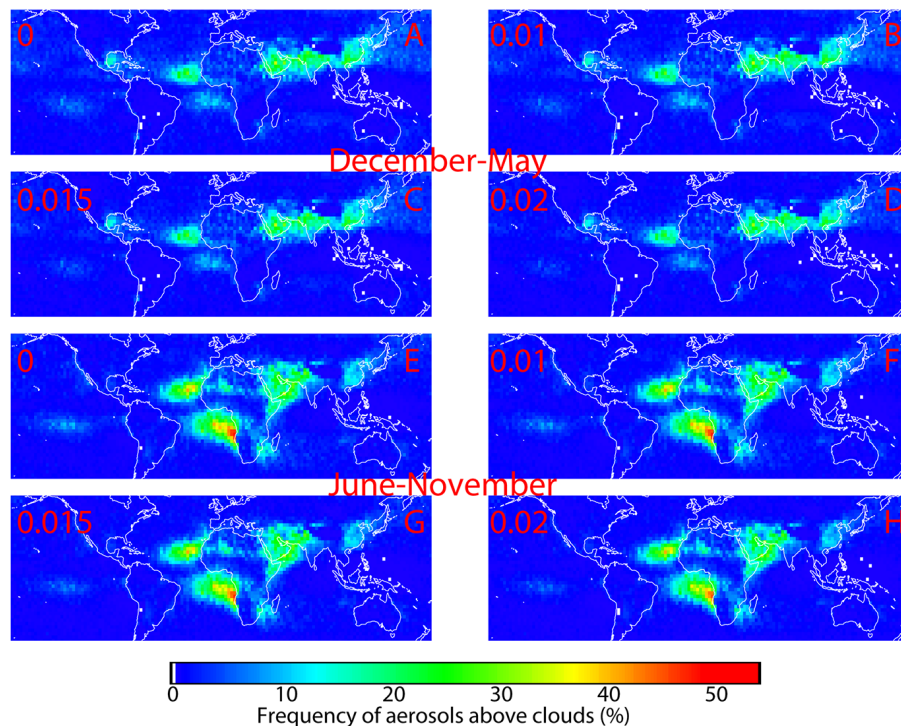


**Figure 2. (a–h)** Multi-year (2006–2013) CALIOP-derived daytime global cloudy-sky ACA frequency applying different CALIOP AODs as the threshold between background and significant aerosol loading. The CALIOP AOD are binned into  $2.5 \times 2.5$  latitude by longitude degree boxes derived using the CALIOP cloud and layer data sets. CALIOP AOD baseline thresholds of 0, 0.010, 0.015 and 0.020 are applied to **(a–d)** respectively for the December–May period. **(e–h)** show the similar results as **(a–d)** but for the June–November period.

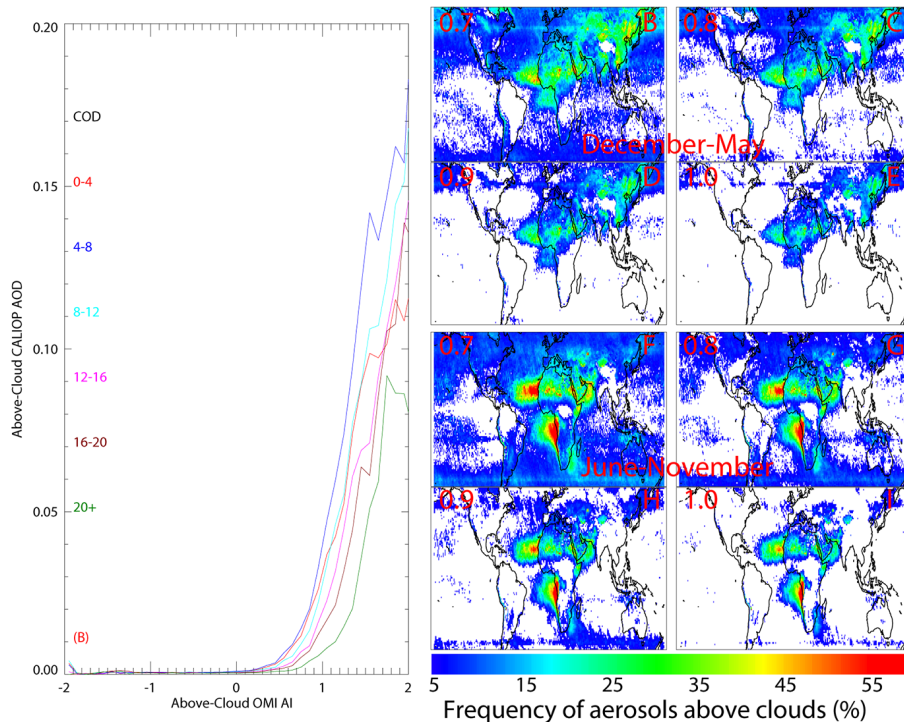


**Figure 3.** (a) Pairwise comparison between collocated OMI and CALIOP observations of above-cloud AI and AOD, respectively, as a function of the underlying MODIS cloud optical depth (COD). CALIOP AOD are averaged into OMI AI bins of 0.1. (b) Multi-year (2006–2013) daytime global cloudy-sky ACA frequency applying several different OMI AIs as the threshold between background and significant aerosol loading. The OMI AIs are binned into  $1^\circ \times 1^\circ$  bins derived from the MODIS-OMI collocated data set. OMI AI baseline thresholds of 0.7, 0.8, 0.9 and 1.0 are applied to Fig. 2c–f respectively for the December–May period. Figure 2f–i depicts the same information as Fig. 2c–f for the June–November period. ACA frequencies less than 5% are shown in white.

Frequency and Trends of Above-Cloud Aerosols

R. Alfaro-Contreras et al.

Title Page

Abstract Introduction

Conclusions References

Tables Figures

◀ ▶

◀ ▶

Back Close

Full Screen / Esc

Printer-friendly Version

Interactive Discussion



## Frequency and Trends of Above-Cloud Aerosols

R. Alfaro-Contreras et al.

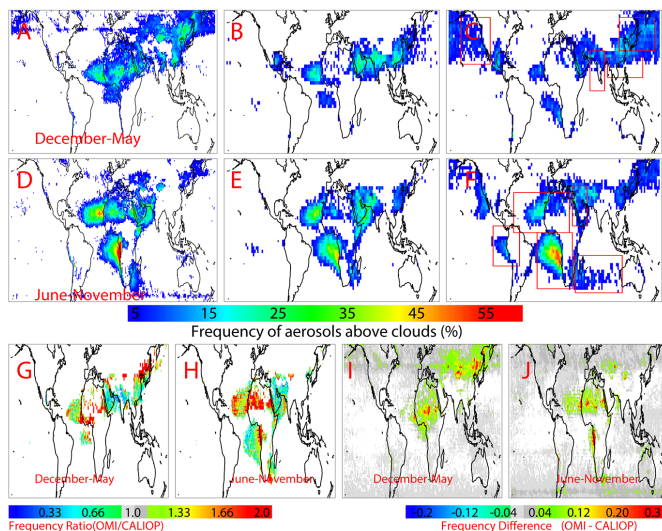


**Figure 4.** (a) Multi-year (December 2006–May 2013) daytime cloudy-sky frequency of occurrence of aerosol above-cloud events during December through May defined from OMI (ratio of opaque MODIS pixels with AI greater than 1.0 to the number of total opaque MODIS pixels). (b) Day-time cloudy-sky frequency of occurrence of above-cloud aerosol events over cloudy skies from CALIOP (ratio of CALIOP pixels with CALIOP  $\text{AOD}_{\text{above cloud}} > 0.015$  to the number of CALIOP pixels with column integrated COD  $> 0$ ) for the same temporal domain as (a). (c) night-time cloudy-sky frequency of occurrence defined similar to the day time frequency from (b). (d–f) show the same information as (a–c) during June 2006–November 2013. (g and h) depict the ACA frequency ratio defined as the OMI-MODIS daytime cloudy-sky frequency divided by the CALIOP derived daytime cloudy-sky frequency for the December to May and June to November period, respectively. (i and j) depict the difference in cloudy-sky frequency used to construct the frequency ratio plots (g and h) for the same temporal ranges. The red boxes show the areas selected for regional studies. Only OMI and CALIOP bins with frequency of 5% or higher are shown in this analysis.

[Title Page](#)
[Abstract](#)
[Introduction](#)
[Conclusions](#)
[References](#)
[Tables](#)
[Figures](#)
[Back](#)
[Close](#)
[Full Screen / Esc](#)
[Printer-friendly Version](#)
[Interactive Discussion](#)



## Frequency and Trends of Above-Cloud Aerosols

R. Alfaro-Contreras et al.

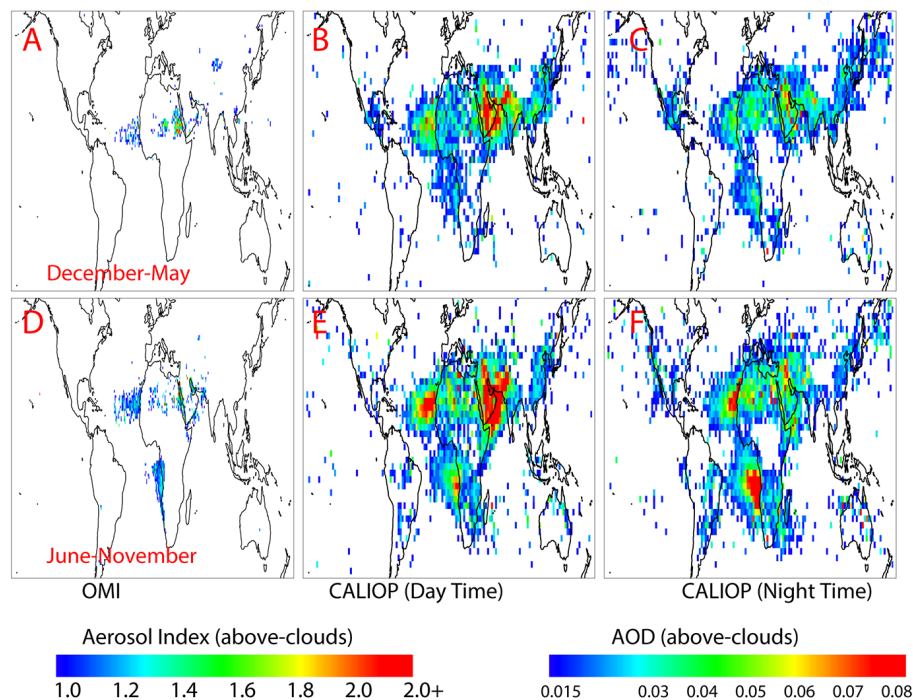


**Figure 5.** (a) Multi-year (2006–2013) daytime Aerosol Index (AI) averaged into  $1.0^\circ \times 1.0^\circ$  bins constructed from collocated MODIS and OMI AI over strictly MODIS cloudy scenes during December through May. The averaged OMI AI is neglected below 1.0 in accordance with the AI ground floor determined in Fig. 3. (b) Multi-year (2006–2013) daytime above-cloud aerosol optical depth (ACAOD) averaged into  $2.5^\circ \times 2.5^\circ$  bins derived from CALIOP cloud and aerosol layer products. Averaged CALIOP ACAOD below 0.015 are considered below the noise floor for the study and thus are not shown. (c) shows the CALIOP ACAOD similar to Fig. 5b except for night-time observations. (d–f) shows the same information as (a–c) during the summer and fall months (June–November).

[Title Page](#)
[Abstract](#)
[Introduction](#)
[Conclusions](#)
[References](#)
[Tables](#)
[Figures](#)
[Back](#)
[Close](#)
[Full Screen / Esc](#)
[Printer-friendly Version](#)
[Interactive Discussion](#)

## Frequency and Trends of Above-Cloud Aerosols

R. Alfaro-Contreras et al.

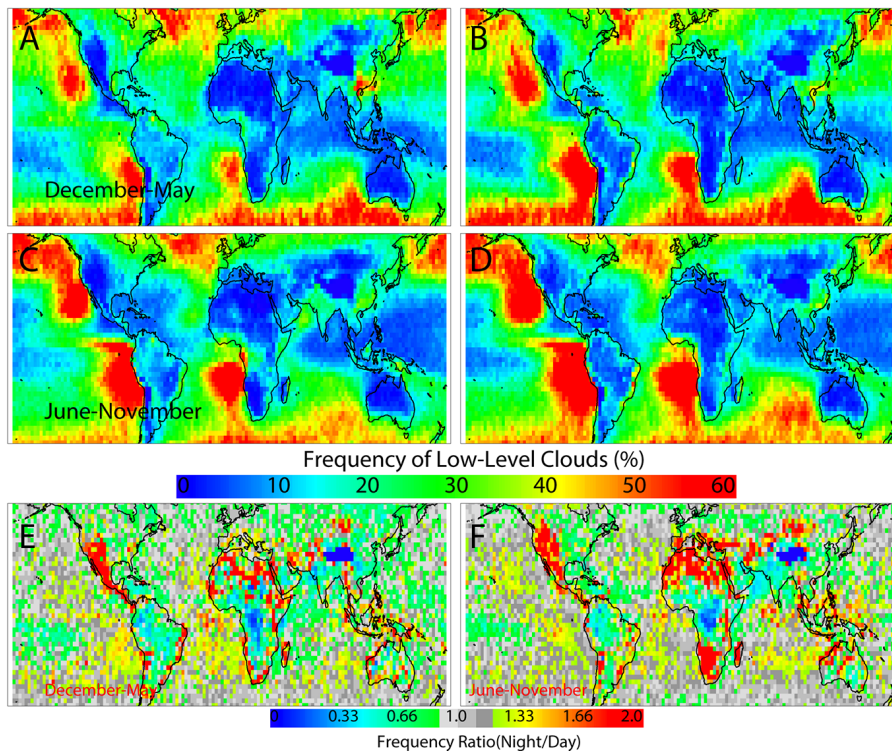


**Figure 6.** Multiyear (June 2006–November 2013) frequency of occurrence of low-level clouds defined by CALIOP as the ratio pixels with COD greater than 0 with cloud-top height < 3 km to the total number of CALIOP scenes within the current  $2.5^\circ \times 2.5^\circ$  bin for (a) December to May during day-time observations. (b) December to May of night-time observations. (c) Daytime frequency of occurrence of low-level cloud decks defined similar to (a) during the June–November time frame and (d). Nighttime frequency of occurrence of low-level cloud decks for the same time frame as (c). (e and f) depict the night to daytime frequency ratio for the December to May and June to November period, respectively.

[Title Page](#)
[Abstract](#)
[Introduction](#)
[Conclusions](#)
[References](#)
[Tables](#)
[Figures](#)
[Back](#)
[Close](#)
[Full Screen / Esc](#)
[Printer-friendly Version](#)
[Interactive Discussion](#)

## Frequency and Trends of Above-Cloud Aerosols

R. Alfaro-Contreras et al.

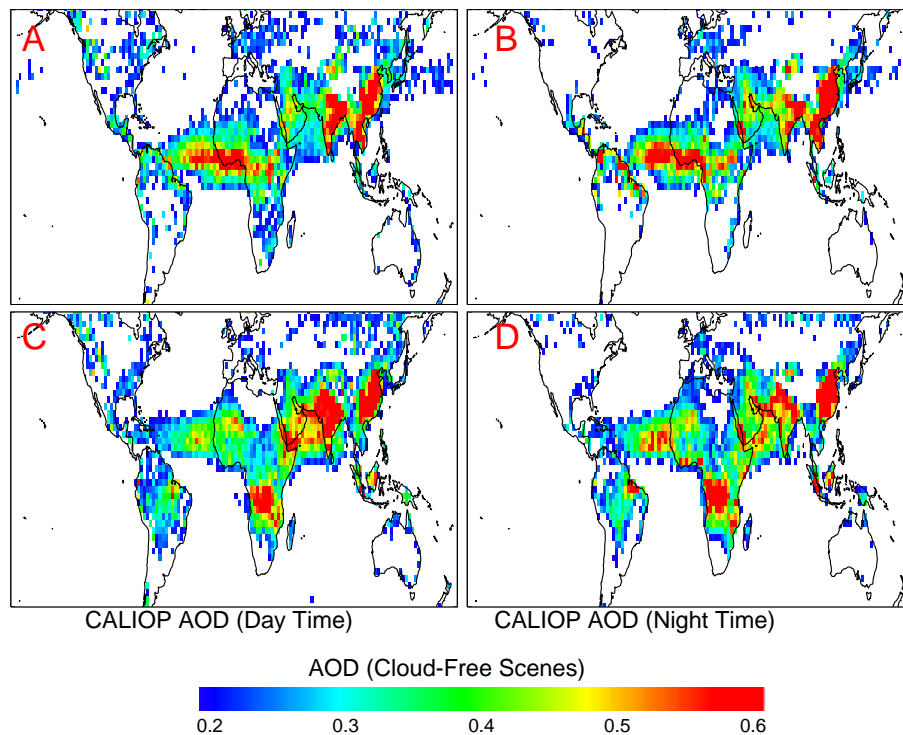


**Figure 7.** (a) Multi-year (2006–2013)  $2.5^\circ \times 2.5^\circ$  averaged CALIOP day-time aerosol optical depth (AOD) for December through May over completely cloud free scenes derived from CALIOP cloud and aerosol layer products for (a) daytime analysis during the December to May period. (b) Nighttime analysis during the December to May period. (c) Daytime analysis for the June to November period and (d) nighttime analysis for the June to November period.

[Title Page](#)[Abstract](#)[Introduction](#)[Conclusions](#)[References](#)[Tables](#)[Figures](#)[◀](#)[▶](#)[◀](#)[▶](#)[Back](#)[Close](#)[Full Screen / Esc](#)[Printer-friendly Version](#)[Interactive Discussion](#)

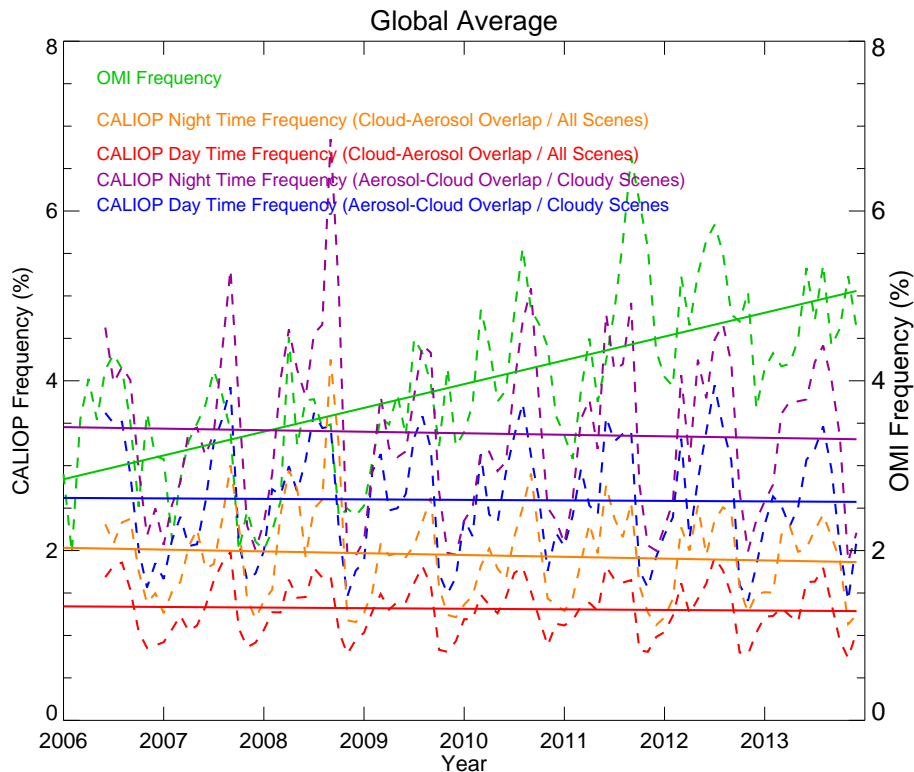


**Figure 8.** Monthly-averaged global ACA frequencies derived using the OMI-MODIS based method (green) as well as CALIOP-based method as described in the text. The corresponding baseline thresholds are applied to both CALIOP and OMI data. Dashed lines represent monthly variations in ACA frequencies where the solid lines represent the yearly ACA frequency trends: OMI daytime cloudy-sky frequency is shown in green, CALIOP nighttime cloudy-sky frequency is purple, CALIOP nighttime all-sky frequency is orange, CALIOP daytime cloudy-sky frequency is blue and CALIOP daytime all-sky frequency is red.

**Frequency and Trends of Above-Cloud Aerosols**

R. Alfaro-Contreras et al.

Title Page	
Abstract	Introduction
Conclusions	References
Tables	Figures
◀	▶
◀	▶
Back	Close
Full Screen / Esc	
Printer-friendly Version	
Interactive Discussion	



## Frequency and Trends of Above-Cloud Aerosols

R. Alfaro-Contreras et al.

Title Page

Abstract

Introduction

Conclusions

References

Tables

Figures

◀

▶

◀

▶

Back

Close

Full Screen / Esc

Printer-friendly Version

Interactive Discussion

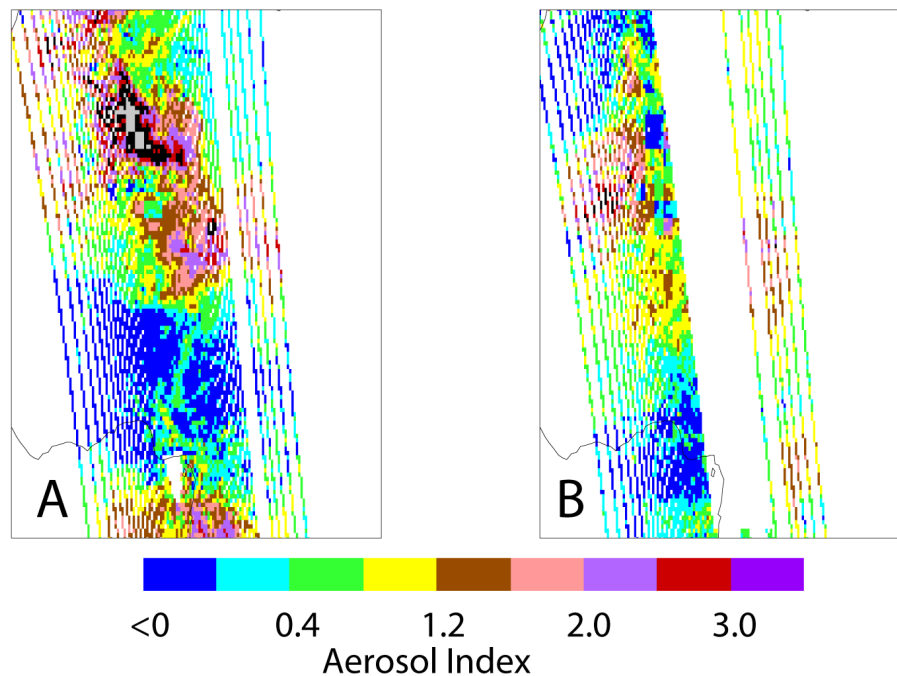


**Figure 9.** (a) A single swath from the OMI instrument over northern Africa on 1 August 2007 before the significant data loss reported in all OMI aerosol products. (b) A single OMI AI swath over the same region as (a) on 1 June 2009 which is affected by the significant data loss.

## Frequency and Trends of Above-Cloud Aerosols

R. Alfaro-Contreras et al.

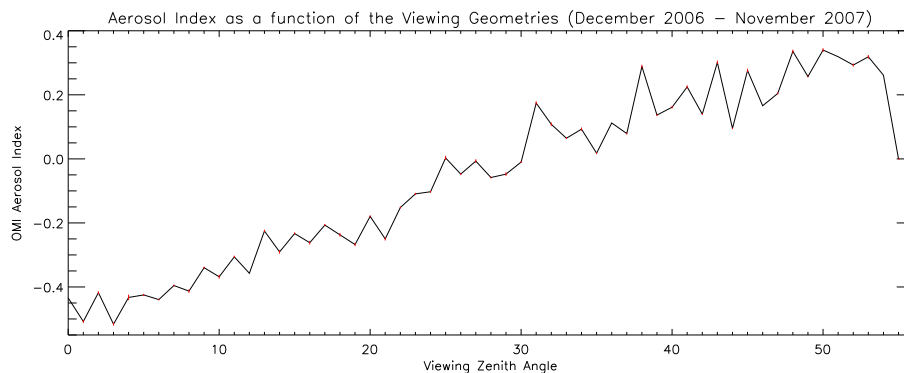


**Figure 10.** The OMI AI as a function of sensor's viewing zenith angle (VZA). All OMI AI data over the course of a year (2007) was binned into  $1^\circ$  VZA increments. The red vertical bars represent the 95 % confidence interval for each  $1^\circ$  bin.

[Title Page](#)[Abstract](#)[Introduction](#)[Conclusions](#)[References](#)[Tables](#)[Figures](#)[◀](#)[▶](#)[◀](#)[▶](#)[Back](#)[Close](#)[Full Screen / Esc](#)[Printer-friendly Version](#)[Interactive Discussion](#)

## Frequency and Trends of Above-Cloud Aerosols

R. Alfaro-Contreras et al.

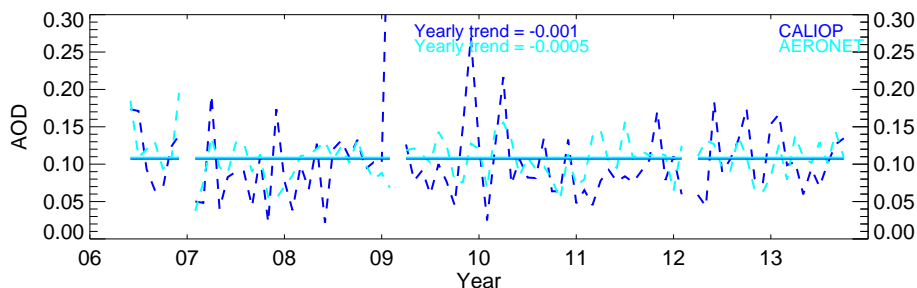


**Figure 11.** Monthly-averaged over ocean clear-sky AODs derived from collocated CALIOP and AERONET data. CALIOP retrievals within  $0.3^\circ$  latitude and longitude and  $\pm 30$  min of the corresponding AERONET station and observation are considered collocated. AERONET and CALIOP AODs above 0.2 and 0.6, respectively, are not included in order to avoid high aerosol loading cases and exclude noisy CALIOP data.

[Title Page](#)[Abstract](#)[Introduction](#)[Conclusions](#)[References](#)[Tables](#)[Figures](#)[◀](#)[▶](#)[◀](#)[▶](#)[Back](#)[Close](#)[Full Screen / Esc](#)[Printer-friendly Version](#)[Interactive Discussion](#)



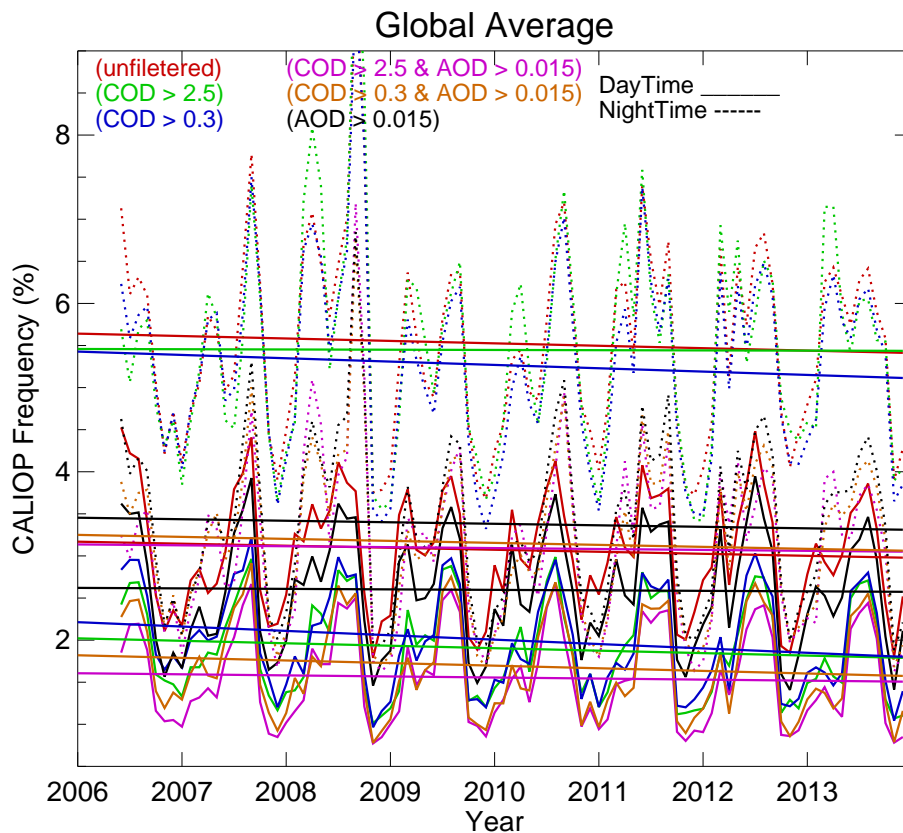


**Figure 12.** Monthly-averaged global CALIOP cloudy-sky frequencies after applying several different threshold techniques to both day and nighttime data. The solid lines show the daytime scenario for each respective case while the dashed lines show the nighttime observations for each case.

**Frequency and Trends of Above-Cloud Aerosols**

R. Alfaro-Contreras et al.

Title Page	
Abstract	Introduction
Conclusions	References
Tables	Figures
◀	▶
◀	▶
Back	Close
Full Screen / Esc	
Printer-friendly Version	
Interactive Discussion	



## Frequency and Trends of Above-Cloud Aerosols

R. Alfaro-Contreras et al.

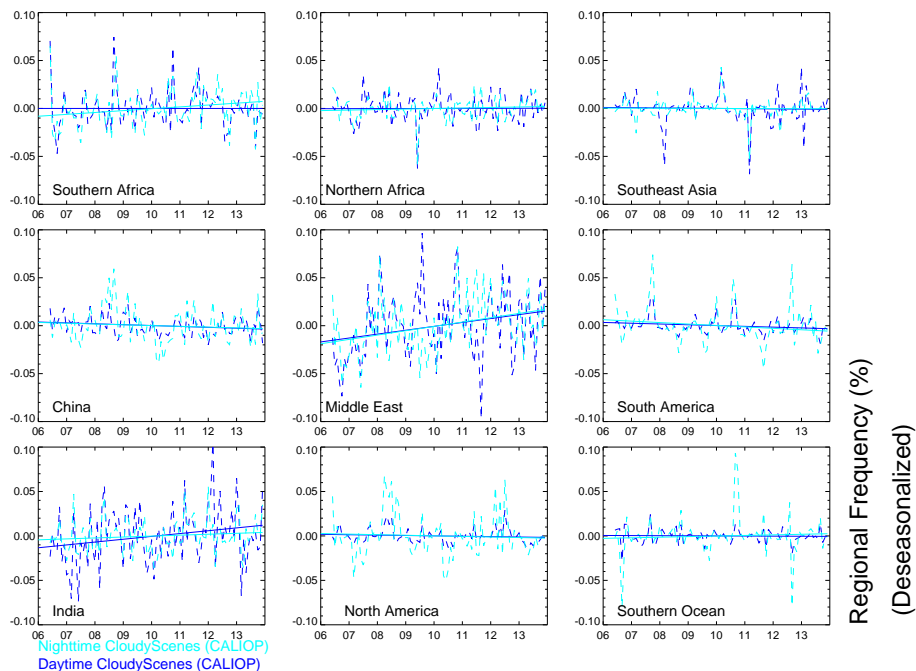


**Figure 13.** The de-seasonalized monthly- and regionally-averaged cloudy-sky frequency of above-cloud aerosol occurrences for the nine different regions outlined in Fig. 4 and explained in Table 1. The dashed lines shows the monthly frequency over the regions while the solid lines show the trend lines computed for each region with the x axis shows represents the year of the study. CALIOP nighttime is shown in aqua marine while the day-time is shown in dark.

[Title Page](#)
[Abstract](#)
[Introduction](#)
[Conclusions](#)
[References](#)
[Tables](#)
[Figures](#)
[Back](#)
[Close](#)
[Full Screen / Esc](#)
[Printer-friendly Version](#)
[Interactive Discussion](#)